


# The effect of A-site cation on ferroelectric properties in $\text{Na}_{0.5}\text{Bi}_{0.5}\text{TiO}_3$ -based materials: Correlation between Burns temperature and remanent polarization

Cite as: J. Appl. Phys. **127**, 144102 (2020); <https://doi.org/10.1063/1.5131201>

Submitted: 12 October 2019 . Accepted: 25 March 2020 . Published Online: 10 April 2020

Krishnarjun Banerjee, and Saket Asthana 



View Online



Export Citation



CrossMark



## Instruments for Advanced Science

Contact Hiden Analytical for further details:

**W** [www.HidenAnalytical.com](http://www.HidenAnalytical.com)

**E** [info@hiden.co.uk](mailto:info@hiden.co.uk)

**CLICK TO VIEW** our product catalogue

**Gas Analysis**

- dynamic measurement of reaction gas streams
- catalysis and thermal analysis
- molecular beam studies
- dissolved species probes
- fermentation, environmental and ecological studies

**Surface Science**

- UHV-TPD
- SIMS
- end point detection in ion beam etch
- elemental imaging - surface mapping

**Plasma Diagnostics**

- plasma source characterization
- etch and deposition process reaction kinetic studies
- analysis of neutral and radical species

**Vacuum Analysis**

- partial pressure measurement and control of process gases
- reactive sputter process control
- vacuum diagnostics
- vacuum coating process monitoring



# The effect of A-site cation on ferroelectric properties in $\text{Na}_{0.5}\text{Bi}_{0.5}\text{TiO}_3$ -based materials: Correlation between Burns temperature and remanent polarization

Cite as: J. Appl. Phys. 127, 144102 (2020); doi: 10.1063/1.5131201

Submitted: 12 October 2019 · Accepted: 25 March 2020 ·

Published Online: 10 April 2020



View Online



Export Citation



CrossMark

Krishnarjun Banerjee and Saket Asthana<sup>a)</sup>

## AFFILIATIONS

Advanced Functional Materials Laboratory, Department of Physics, Indian Institute of Technology Hyderabad, Kandi, Telangana 502285, India

<sup>a)</sup>Author to whom correspondence should be addressed: [asthanas@iith.ac.in](mailto:asthanas@iith.ac.in). Tel.: (+91) 040 2301 6067

## ABSTRACT

The effect of cation radius mismatch on the relaxor to paraelectric state transition temperature of the lead free ferroelectric  $\text{Na}_{0.5-x}\text{Rb}_x\text{Bi}_{0.5}\text{TiO}_3$  was examined, and the observed trend was different from manganite perovskites. The transition temperatures of these compounds were estimated from the temperature dependent dielectric curves. The nature of the dielectric curve at the transition temperature was broad unlike a normal ferroelectric. The dependency of the transition temperature on the A-site cation radius mismatch was explained through the correlation among polarizations of the polar nanoregions (PNRs). An asymmetric nature in the imaginary part of the impedance spectra was observed for the composition with higher disorder at the A-site, which is attributed to the relaxation time distribution of the PNRs. The decrement in the value of remanent polarization ( $P_r$ ) with the increment in A-site substitution was also noticed. A relationship between the transition temperature from the relaxor to paraelectric state and  $P_r$  of the A-site disorder  $\text{Na}_{0.5}\text{Bi}_{0.5}\text{TiO}_3$ -based systems was attempted to be established.

Published under license by AIP Publishing. <https://doi.org/10.1063/1.5131201>

## I. INTRODUCTION

The dielectric and the ferroelectric properties of the  $\text{ABO}_3$  type perovskite material can be tuned by the substitution of different cations or the amount of the substituents at the A- and B-sites. Usually, chemical compositions, structure, tolerance factor, masses, and charges of the A- and B-site cations are considered important factors to tailor the properties of a ferroelectric material. The size of the cations and their distribution at the particular site are pertinent parameters that are less documented in the literature. The size mismatch modulates the physical properties of the material as the mean cation radius changes with the percentage of the substituent, and the mean cation radius directly influences the tolerance factor. The relation between the tolerance factor ( $t$ ) and the mean cation radius at A-site ( $\langle r_A \rangle$ ) is defined as

$$t = \frac{\langle r_A \rangle + r_O}{\sqrt{2}(r_B + r_O)}, \quad (1)$$

where  $r_O$  and  $r_B$  are the radii of the O ion and the B-site cation, respectively. Rodriguez-Martinez and Attfield observed the dependency of the transition temperature of the ferromagnetic metallic to paramagnetic insulating state ( $T_m$ ) on the mean radius of the A-site cation in the  $\text{R}_{0.7}\text{M}_{0.3}\text{MnO}_3$  (where R = La, Pr, Nd, Sm and M = Ca, Sr, Ba) perovskite.<sup>1</sup> They studied the random distribution of  $\text{R}^{3+}$  and  $\text{M}^{2+}$  cations with different ionic radii at the A-site and quantified it by using the concept of size variance ( $\sigma^2$ ), which is defined as

$$\sigma^2 = \sum_i x_i r_i^2 - \langle r_A \rangle^2, \quad (2)$$

where  $r_i$  and  $x_i$  are the ionic radii and fractional occupancy of the A-site cations, respectively. A linear relationship is observed between  $T_m$  and  $\sigma^2$  (below  $0.015 \text{ \AA}^2$ ) for manganite perovskites and  $T_m$  decreases with increasing  $\sigma^2$ . The reason behind such behavior is the creation of additional displacement of  $\text{O}^{2-}$  because

of the size mismatch at the A-site and the generation of strain energy in the unit cell of the perovskite structure.<sup>1</sup> The linear equation, which is followed by the experimental data, is given by

$$T_m(\langle r_A \rangle, \sigma^2) = T_m(\langle r_A \rangle, 0) - p_1 \sigma^2, \quad (3)$$

where  $p_1 \approx \frac{K}{\Delta S_m}$ ,  $K$  is the force constant of the Mn–O bond and  $\Delta S_m$  is the change in entropy at transition. The A-site cation disorder tunes not only the transition temperature of manganites but also that of ferroelectric materials. Sinclair and Attfield showed the linear increment of Curie temperature ( $T_c$ ) with the increase in disorder at the A-site of  $\text{Ba}_{1-x}\text{Ca}_x\text{TiO}_3$ .<sup>2</sup> A-site size variance also alters the characteristic features of the ferroelectric material, which is noticed in Ca and Ba doped  $\text{SrTiO}_3$ .<sup>3</sup> The increment in  $T_c$  with the increment in  $\sigma^2$  and  $\langle r_A \rangle$  is also found in the  $\text{Ba}_{1-x-y}\text{Sr}_x\text{Ca}_y\text{TiO}_3$  systems.<sup>4</sup> One should note that the aforementioned inspected ferroelectric compounds are the normal ferroelectric materials (NFs). In the case of  $\text{BaTiO}_3$ -based compositions, the ferroelectric to paraelectric transitions are almost sharp and the transition temperatures are easily determinable, but the scenario is quite intriguing for a ferroelectric with diffused phase transition or a relaxor ferroelectric with diffused phase transition. It is well known that the relaxor ferroelectric materials (RFs) have a broad transition in the vicinity of  $T_m$  (temperature at the maximum dielectric constant) and the paraelectric state occurs above the Burns temperature ( $T_B$ ). The dielectric curve of RFs also shows frequency dispersion, which is contrary to the property of the NFs. It is always the matter of interest to know the variation of the dielectric and ferroelectric properties of the RFs, because RFs become superior over NFs due to their excellent properties and applicability. Specifically, lead free RFs have attained more importance because of their non-toxic nature and other features like high dielectric constant, good thermal stabilization, high piezoelectric constant, electrostriction, recoverable energy storage density, etc., which are desired properties to make the materials suitable for various practical applications. As discussed earlier, unlike the  $T_c$  of NFs, the RFs transform to the paraelectric state above  $T_B$ . The higher  $T_B$  and the thermal stability of the dielectric constant (almost constant dielectric constant value and broad transition with respect to temperature) secure the RFs for high temperature applications. In this work, the lead free  $\text{Na}_{0.5}\text{Bi}_{0.5}\text{TiO}_3$  (NBT) with the substitution of Rb at the A-site is chosen for the study. This system is selected because of its diffused type phase transition and dispersive nature of the dielectric constant, which may help us to understand the influence of A-site cation size disparity on the properties of the lead free RFs.<sup>5</sup> Another reason for selecting this material is due to the higher size mismatch that creates more disorder at the A-site (the radii of the  $\text{Na}^{1+}$ ,  $\text{Bi}^{3+}$ , and  $\text{Rb}^{1+}$  ions are 1.39, 1.40, and 1.74 Å, respectively, in the 12-fold coordination). In this work, the dependency of the diffused type phase transition and  $T_B$  on  $\sigma^2$  is discussed in the first part. The broadness of the dielectric curve at  $T_m$  is explained through the interaction among the polar nanoregions (PNRs) for high and low values of  $\sigma^2$ . Furthermore, the presence of PNRs and their relaxation time distribution is analyzed by the conventional impedance technique, which is discussed in the second part. The motivation behind the study on such series arises due to their potential applications in the field of energy storage and medical implants. At room temperature, the calculated recoverable energy storage density

of 4 mol. % Rb substituted NBT is  $0.71 \text{ J/cm}^3$ .<sup>5</sup> This value is larger than some of the A-site disorder  $\text{Na}_{0.5}\text{Bi}_{0.5}\text{TiO}_3$  ferroelectrics and  $\text{Na}_{0.5}\text{Bi}_{0.5}\text{TiO}_3$ -based solid solutions. Moreover, the same composition is bio-compatible with high hardness. These properties show better suitability of RB4 over traditional ceramics ( $\text{Al}_2\text{O}_3$ ) for orthopedic implants. The piezoelectric property of RB4 will support to monitor the failure of the implant non-invasively and avoid reverse surgery. This material can show the pathway to use an eco-friendly piezo-implant instead of lead-based material embedded implants.<sup>5</sup>

It is obvious that the mismatch of the A-site cation radii also modulates the polarization of a ferroelectric material, as it creates distortion in the  $\text{BO}_6$  octahedra.<sup>1</sup> The situation is illustrated schematically according to the hard sphere model in Figs. 1(a) and 1(b). Figure 1(a) depicts a cubic perovskite ( $\text{ABO}_3$ ) in which the A-site is occupied by cations “ $A_0$ ” with radii “ $a_0$ .” In this system, due to the occupancy of same size and same type of cations at the A-site, there is no size disorder at this site, and the value of  $\sigma^2$  becomes zero [Eq. (2)]. Now, a cation “A” with radius larger than  $a_0$  is substituted at the A-site, which causes displacement of  $\text{O}^{2-}$ , and it modulates the  $\text{BO}_6$  octahedra [Fig. 1(b)].<sup>1,6</sup> The deformation of the  $\text{BO}_6$  octahedra is able to alter the polarization property of the ferroelectric materials. Since  $T_B$  is also affected by the radius mismatch, we propose that there should be a well defined relationship between  $T_B$  and remanent polarization ( $P_r$ ) for the RFs. In Sec. III C,  $T_B$  and  $P_r$  of some lead free A-site disordered ferroelectrics are collected and the relationship is established.

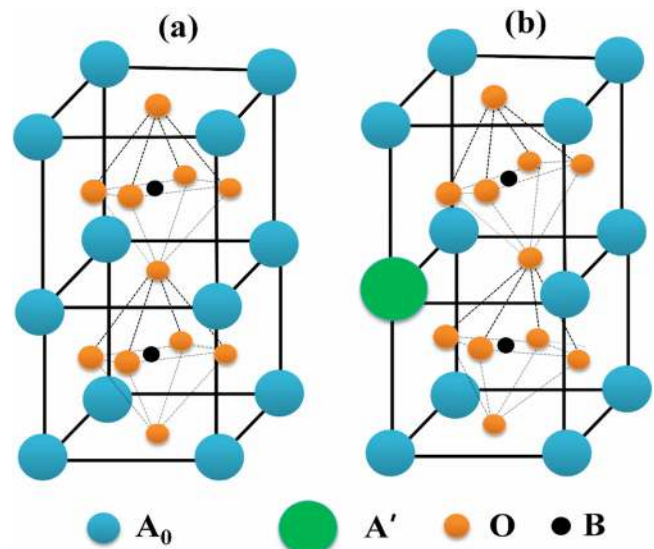


**FIG. 1.** A diagram of a perovskite ( $\text{ABO}_3$ ) structure with two unit cells. The positions of the A-site cation, B-site cation, and  $\text{O}^{2-}$  are shown at the corner, body center, and phase center of the unit cell, respectively. (a) The picture represents that both unit cells contain A-site cations “ $A_0$ ” of radii  $a_0$  with the undistorted  $\text{BO}_6$  octahedra. For this structure, the value of  $\sigma^2$  is zero. (b) The effect of the cation size mismatch is shown in this picture. The  $\text{BO}_6$  octahedra of the unit cells are distorted due to the substitution of a bigger cation “A” at the A-site.

## II. EXPERIMENTAL SECTION

$\text{Na}_{0.5-x}\text{Rb}_x\text{Bi}_{0.5}\text{TiO}_3$  ( $x = 0, 1, 2, 3,$  and  $4$  mol. %, abbreviated as RB0, RB1, RB2, RB3, and RB4, respectively, in this article) were prepared by the solid state sintering technique.  $\text{Na}_2\text{CO}_3$ ,  $\text{Bi}_2\text{O}_3$ ,  $\text{TiO}_2$ , and  $\text{Rb}_2\text{CO}_3$  (99.99%, Sigma Aldrich Chemicals, USA) powders were used as the precursors. The dried powders were weighed carefully according to the mol. % ratio and mixed properly. The calcination is done at  $800^\circ\text{C}$  for 3 h. After adding the binder, powders were granulated and pressed into circular disks of 8 mm diameter. The green pellets are sintered at  $1150^\circ\text{C}$  for 3 h. The phase formation was confirmed from the x-ray diffraction patterns of the prepared samples by using an x-ray diffractometer (PANalyticalX'pert pro) at room temperature. The presence of grins and their size variation for all compositions were observed in a field emission scanning electron microscope (Zeiss, Supra 40); the data were reported in our previous article.<sup>5</sup> The dielectric and impedance study of the samples with the conducting layer was performed by using the impedance analyzer attached with an oven (Wayne Kerr 6500B). The polarization measurement of the samples is done in the TF-Analyzer 2000 (aixACCT systems GMBH) at 1 Hz and room temperature.

## III. RESULTS AND DISCUSSION

### A. Effect of the cation size variance on the Burns temperature

One of the important consequences of substitution at the A-site of the  $\text{ABO}_3$  type structure is size variance at that site. The mean radius of the A-site cation (denoted as  $\langle r_A \rangle$ ) changes with different substituents and their concentrations. In our present study, statistically it is not erroneous to think that  $\text{Na}^{1+}$ ,  $\text{Bi}^{3+}$ , and  $\text{Rb}^{1+}$  are randomly distributed at the A-site with different radii. The concept of variance ( $\sigma^2$ ) is an essential parameter to quantify the dispersion of the distribution of the radii from the mean value. In the case of the A-site disorder perovskite, the variance can be written as

$$\sigma^2 = \sum_i x_i r_i^2 - \langle r_A \rangle^2, \quad (4)$$

where  $r_i$  and  $x_i$  are the ionic radii and fractional occupancy of the A-site cations, respectively. For the Rb substituted  $\text{Na}_{0.5}\text{Bi}_{0.5}\text{TiO}_3$  [ $\text{Na}_{(0.5-x)}\text{Rb}_x\text{Bi}_{0.5}\text{TiO}_3$ ], the variance is calculated for each composition, and its variation with respect to  $x$  is depicted in Fig. 2. From our previous study, it has been observed that the transition temperature varies with the substitution of Rb, and there is no particular ferroelectric to paraelectric transition temperature of RB1, RB2, RB3, and RB4.<sup>5</sup> For these type of materials, the ferroelectric to paraelectric transition can be identified from the Burns temperature ( $T_B$ ); below this temperature, the polar nanoregions (PNRs) start to nucleate. In the paraelectric state, the real part of permittivity ( $\epsilon'$ ) obeys the Curie–Weiss law, which is

$$\epsilon' = C/(T - T_{\text{CW}}), \quad (5)$$

where  $C$  is the Curie–Weiss constant and  $T_{\text{CW}}$  is the Curie–Weiss temperature.

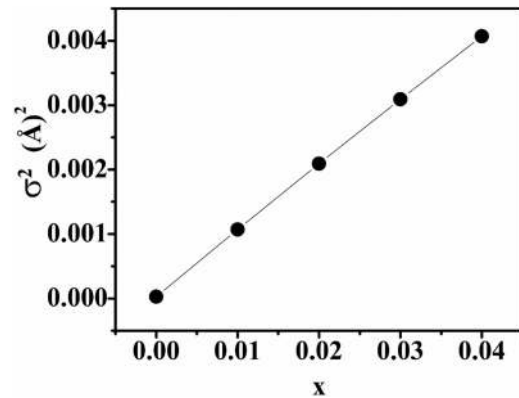
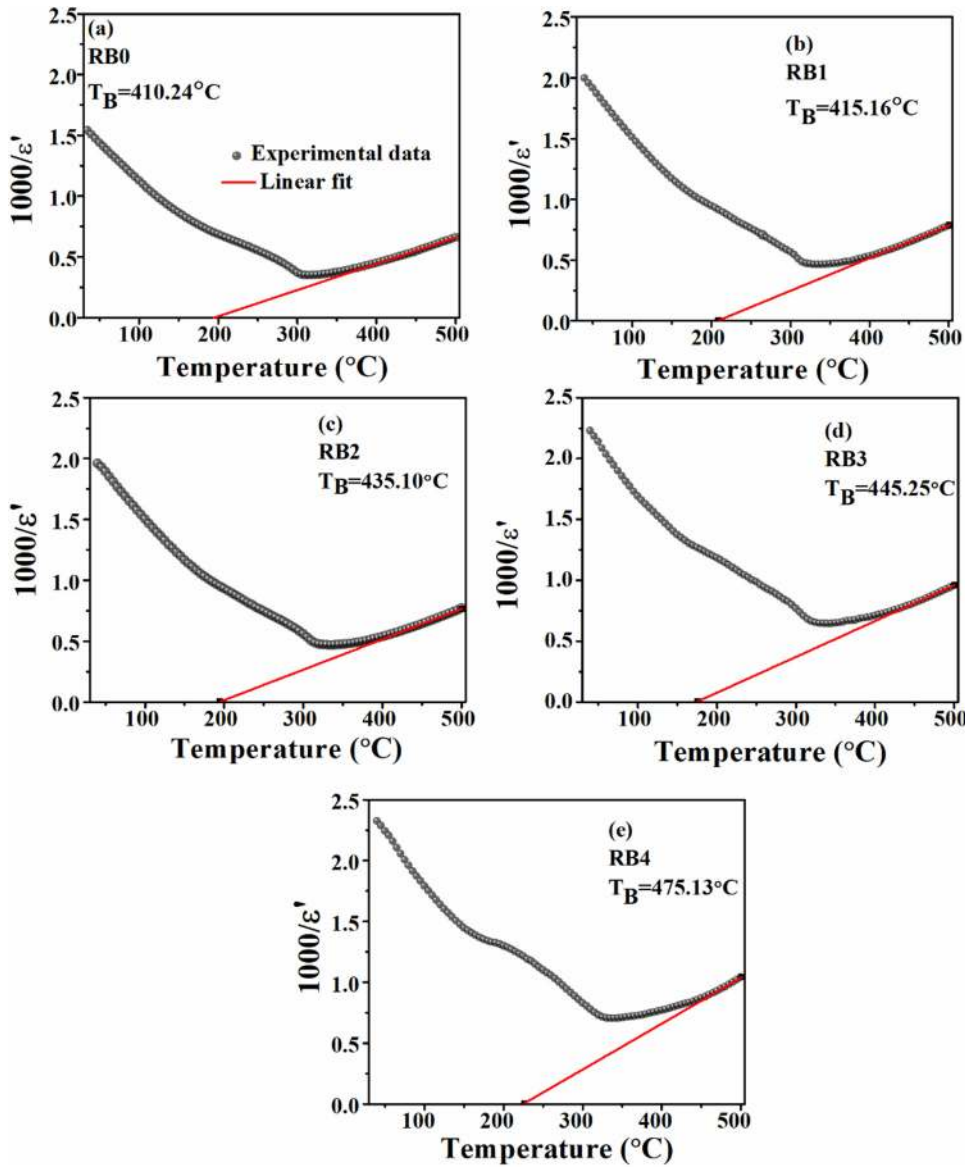


FIG. 2. The linear variation of  $\sigma^2$  with  $x$  for the  $\text{Na}_{(0.5-x)}\text{Rb}_x\text{Bi}_{0.5}\text{TiO}_3$  series, where  $x = 0, 0.01, 0.02, 0.03,$  and  $0.04$ .

Figure 3 shows the temperature dependent  $1000/\epsilon'$  graphs for RB0, RB1, RB2, RB3, and RB4.  $T_B$  of the RFs is designated as a transition temperature, at which the inverse of the real part of the permittivity deviates from the Curie–Weiss law. As shown in Fig. 3, the concentration of  $\text{Rb}^{1+}$  affects  $T_B$ ; in other words,  $T_B$  is tuned by  $\sigma^2$ , because  $\sigma^2$  varies with the concentration of  $\text{Rb}^{1+}$ . To seek the effect of  $\sigma^2$  on the transition temperature, the  $T_B$  values of various compositions are plotted with respect to  $\sigma^2$ , which is shown in Fig. 4. Here, we can note that no linear relationship between  $T_B$  and  $\sigma^2$  is observed in our examined compositions, which is different from  $\text{BaTiO}_3$ -based compositions. Second,  $T_B$  increases with the increase in  $\sigma^2$ , which is completely different from manganese materials.<sup>1</sup> These observations seek better investigations that can explain the effect of  $\sigma^2$  on  $T_B$ . Usually, the creation of dipoles, ferroelectric to paraelectric transition, and other properties of the ferroelectric material are usually explained on the basis of distortion in the geometry of the  $\text{BO}_6$  octahedra of  $\text{ABO}_3$ . One of the most common distortions in the  $\text{BO}_6$  octahedra is associated with the displacement of the B-site cation from the center of the octahedra. Another type of distortion is associated with the rotation/tilt of the  $\text{BO}_6$  octahedra. The  $\text{BO}_6$  octahedron distortion leads to structural phase transition in the ferroelectrics. The ferroelectric property can be altered with the inclusion of a larger size cation at the A-site as it affects the rotation/tilt of the  $\text{BO}_6$  octahedron. In this study, the substitution of  $\text{Rb}^{1+}$  at the A-site of the NBT lattice influences the rotation/tilt of the  $\text{TiO}_6$  octahedron. The higher radius of  $\text{Rb}^{1+}$  at the A-site creates an additional displacement to  $\text{O}^{2-}$ ; the situation is illustrated in Fig. 1(b). The transition temperature for a perovskite material with no cation size mismatch at the A-site is written as<sup>6</sup>

$$T = \frac{\Delta H}{\Delta S}, \quad (6)$$

where  $\Delta H$  and  $\Delta S$  denote the change in transition enthalpy and entropy, respectively.  $\Delta H$  is expressed in terms of mean squared



**FIG. 3.** The temperature dependent  $1000/\epsilon'$  graphs of (a) RB0, (b) RB1, (c) RB2, (d) RB3, and (e) RB4 compositions. The inverse of the real part of the permittivity curve deviates from the Curie–Weiss law at a certain temperature, which is known as the Burns temperature ( $T_B$ ).

displacement of  $O^{2-}$  ( $\langle Q_m^2 \rangle$ ) as follows:

$$\Delta H = \Delta H' + \frac{NK}{2} \langle Q_m^2 \rangle, \quad (7)$$

where the second term on the right-hand side denotes the energy associated with the displacement of  $O^{2-}$  at transition.  $\Delta H'$  is the enthalpy associated with the contributions from electrons, phonons, etc.  $K$  is the mean force constant of the Ti–O bond and  $N$  is the number of bonds (i.e., 6). Now, the additional displacement of  $O^{2-}$  occurs due to the size mismatch at the A-site. In this case, the mean squared displacement of  $O^{2-}$  is denoted as  $\langle Q_d^2 \rangle$ , and the expressions for new transitional enthalpy ( $\Delta H''$ ) and

temperature ( $T''$ ) are as follows:

$$\Delta H'' = \Delta H' + \frac{NK}{2} (\langle Q_m^2 \rangle - \langle Q_d^2 \rangle) = \Delta H - \frac{NK}{2} \langle Q_d^2 \rangle \quad (8)$$

and

$$T'' = \frac{\Delta H''}{\Delta S} = \frac{\Delta H}{\Delta S} - \frac{NK}{2\Delta S} \langle Q_d^2 \rangle = T - \frac{NK}{2\Delta S} \langle Q_d^2 \rangle, \quad (9)$$

where

$$\langle Q_d^2 \rangle = C [\sigma^2 + (r_A^0 - \langle r_A \rangle)^2]. \quad (10)$$

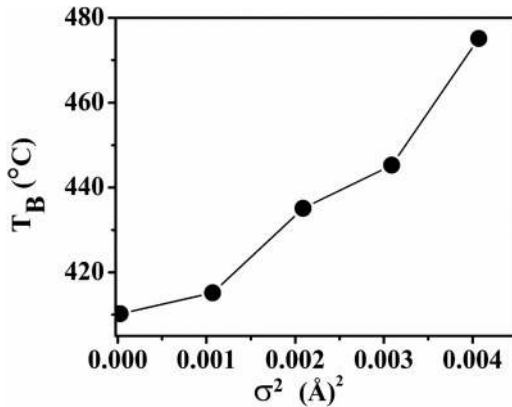


FIG. 4. The plot of the variation of  $T_B$  with  $\sigma^2$ .  $T_B$  increases with the increase in  $\sigma^2$ .

Here,  $r_A^0$  is the radius of the A-site cation of the undistorted perovskite and  $C$  is a constant and its value lies between 0 and 2. One can find the details of this derivation in Ref. 6. The calculated value of  $\langle Q_d^2 \rangle$  for RB0 (or pure NBT) is 1.904 C and for RB4 is 1.945 C. The value of  $\langle Q_d^2 \rangle$  increases with the concentration of Rb in the A-site, which causes the increment in strain energy, and consequently, the transition temperature decreases [Eqs. (8) and (9)]. According to the above explanation, the transition temperature from the relaxor ferroelectric to paraelectric state (or  $T_B$ ) of the relaxor ferroelectric should decrease with the increase in  $\sigma^2$ . However, an opposite scenario is observed in the present system;  $T_B$  increases with the substitution of Rb. The increment can be explained through the enhanced correlation among polarizations of PNRs instead of enhanced strain energy. The local compositional disorder at the A-site leads to the formation of PNRs. The presence of PNRs is evidenced from the temperature dependent dielectric curve at different frequencies. These PNRs have different compositions and local Curie temperatures.<sup>7,8</sup> According to the dipolar glass model, interactions among the dipole moments of the PNRs occur in the relaxor ferroelectric. The fluctuation of the polarization of PNRs between the polarization states increases with the temperature. At lower temperatures ( $\leq T_B$ ), PNRs polarize the neighboring PNRs up to its correlation length ( $r_c$ ).<sup>9</sup> At the temperature below  $T_B$ , the  $r_c$  increases, and the interaction among the PNRs also increases. At and above  $T_m$  (temperature at maximum dielectric constant), the thermal fluctuation becomes higher, and above  $T_B$ , there is no correlation exist among polarizations of the PNRs.<sup>10</sup> The correlations can be estimated from the order parameter “ $q$ .” Sherrington and Krikpatrick have introduced an order parameter “ $q$ ” for the spin glass system, where the spins are interacted through infinite-ranged interactions.<sup>11</sup> Viehland *et al.* calculated the order parameter for  $\text{PbMg}_{1/3}\text{Nb}_{2/3}\text{O}_3$  (PMN) and showed the correlation between polarizations of the polar regions. “ $q$ ” can be derived from susceptibility as follows:<sup>12</sup>

$$\chi = \frac{C[1 - q(T)]}{T - \Theta[1 - q(T)]}, \quad (11)$$

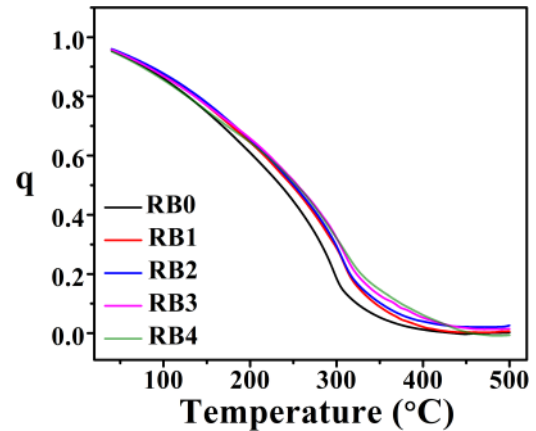


FIG. 5. The plot of the temperature dependent order parameter ( $q$ ) of all compositions. The correlations among the PNRs for RB4 decrease to zero at higher temperature than RB0.

where  $C$  is the Curie constant,  $T$  is the temperature, and  $\Theta$  is the Curie temperature.

$q$  values of all compositions are calculated from the temperature dependent susceptibility at 1 MHz frequency. The temperature dependent “ $q$ ” values of all compositions are plotted in Fig. 5. The diffused phase transition, the presence of  $T_B$ , and deviation of the  $\epsilon'$  curve from the Curie–Weiss law in  $\text{Na}_{0.5-x}\text{Rb}_x\text{Bi}_{0.5}\text{TiO}_3$  compositions allow us to use the equation and establish the correlation among polarization of the PNRs. RB4 has a larger “ $q$ ” value, and it becomes zero gradually at a higher temperature than RB0 as shown in Fig. 5. This infers that the interactions among the polar regions persist up to a higher temperature, and as a result,  $T_B$  is found to be higher in RB4. It should be noted that, above 480  $^{\circ}\text{C}$ , the correlation among the polarizations of PNRs is disrupted due to higher thermal energy. The enhanced correlation in RB4 is the consequence of the local compositional disorder at the A-site of RB4 due to the different sizes of  $\text{Na}^{1+}$ ,  $\text{Bi}^{3+}$ , and  $\text{Rb}^{1+}$  and the higher percentage of  $\text{Rb}^{1+}$ . Along with the increase in  $T_B$  and A-site cation disorder, the transition in the vicinity of  $T_m$  also becomes broader or the transition becomes diffusive, which is not observed in the case of  $\text{BaTiO}_3$ , where the A-site is occupied by the same type of cations. A few equations are available to determine the diffuseness of the dielectric curve. The quadratic equation for the relaxor ferroelectric with diffusive phase transition can be expressed as follows:<sup>7,8,13,14</sup>

$$\frac{\epsilon_m}{\epsilon} = 1 + \frac{(T - T_m)^2}{2\delta_m^2}, \quad (12)$$

where  $\epsilon_m$  is the real part of permittivity at temperature  $T_m$  and  $\delta_m$  denotes the diffuseness of dielectric permittivity. This “quadratic law” expresses the Gaussian distribution of the Curie temperatures of the relaxors in the vicinity of  $T_m$  with standard deviation  $\delta$ .<sup>13</sup> Uchino and Nomura generalized the above equation by using a

critical exponent  $\gamma$  instead of 2,<sup>8</sup>

$$\frac{1}{\epsilon} - \frac{1}{\epsilon_m} = \frac{(T - T_m)^\gamma}{C'} \quad (13)$$

The exponents' values become 1.08 for BaTiO<sub>3</sub> (sharp transition) and 1.76 for Pb(Zn<sub>1/3</sub>Nb<sub>2/3</sub>)O<sub>3</sub> (diffused transition).<sup>8</sup> Researchers commonly determine the diffuseness through  $\gamma$  by using the above equation [Eq. (13)], but sometimes this method is problematic.<sup>15,16</sup> As stated earlier, the most useful parameter that is used to determine the diffuseness is  $\delta$ , but its value also depends on the applied frequency.<sup>13</sup> Bokov and Ye established a modified

equation, with the diffuseness parameter  $\delta_A$ , which is independent of temperature and frequency. The equation is as follows:<sup>13</sup>

$$\frac{\epsilon_A}{\epsilon} = 1 + \frac{(T - T_A)^2}{2\delta_A^2}, \quad (14)$$

where  $T_A < T_m$  and  $\epsilon_A > \epsilon_m$ . The real part of permittivity of the compositions is fitted by the above equation, and  $\delta_A$  is obtained at temperature above  $T_m$  as shown in Fig. 6. The obtained values of  $\delta_A$  for RB0, RB1, RB2, RB3, and RB4 are  $157.23 \pm 1.17$  K,  $163.01 \pm 0.09$  K,  $166.56 \pm 0.7$  K,  $189.23 \pm 0.06$  K, and  $191.01 \pm 0.17$  K, respectively. The higher concentration of Rb significantly affects the

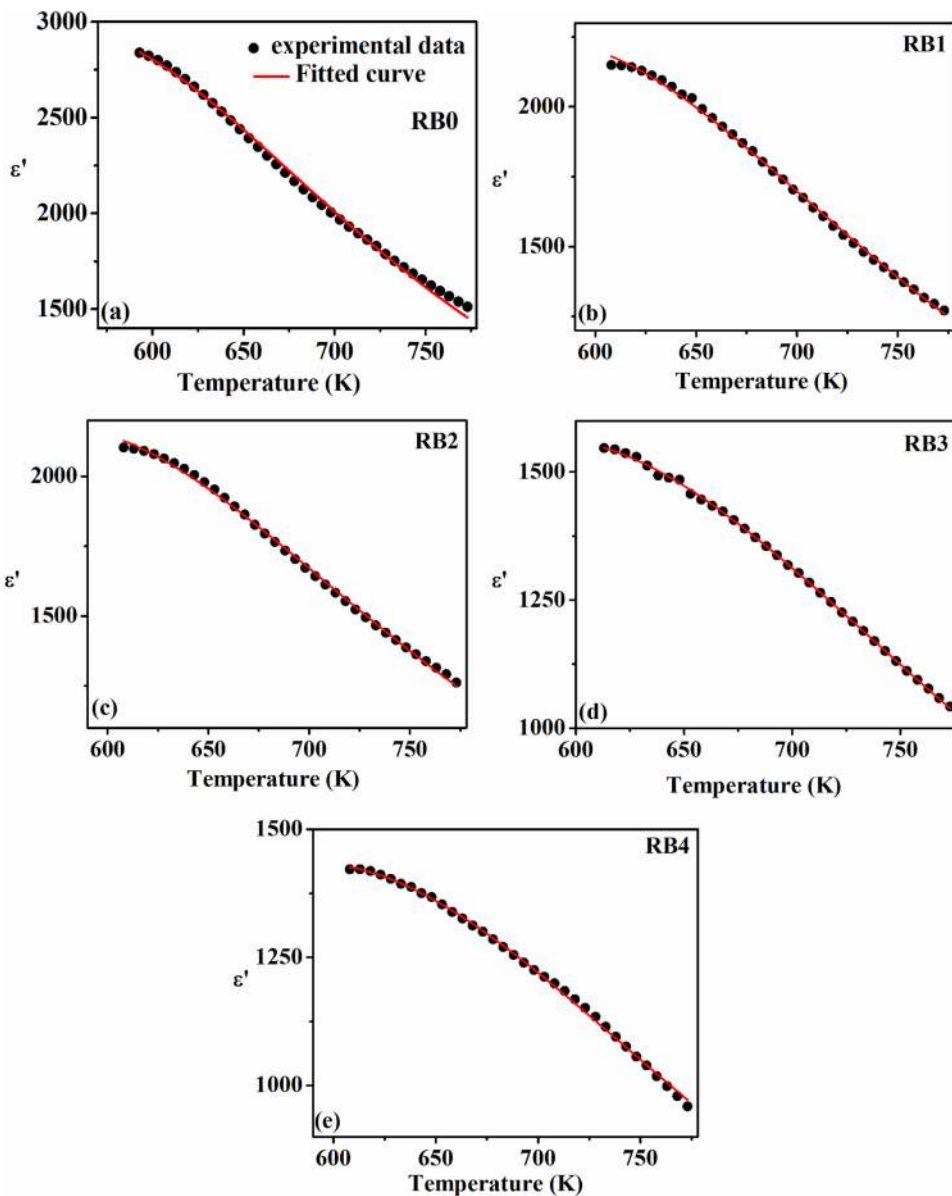


FIG. 6. The graphs of the temperature dependent real part of permittivity above  $T_m$  of (a) RB0, (b) RB1, (c) RB2, (d) RB3, and (e) RB4 compositions. The observed curve is fitted by Eq. (11), and the values of  $\delta_A$  are obtained for all compositions.

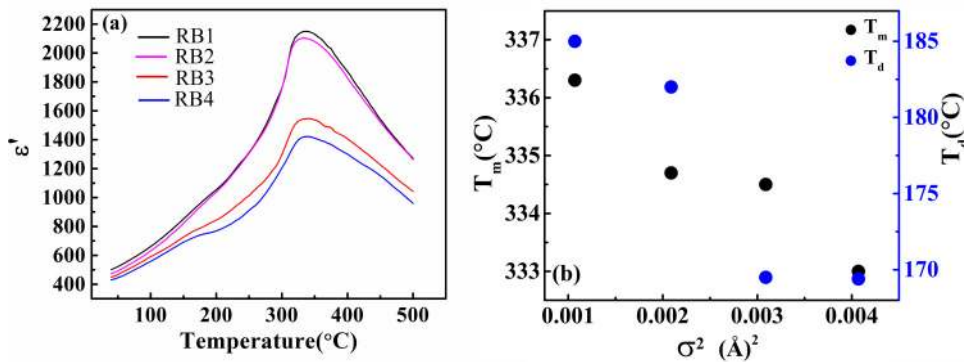


FIG. 7. The graph of the temperature dependence of (a) dielectric constant and (b) the variation of  $T_m$  and  $T_d$  of all compositions with the cation size variance.

peak width at the temperature around  $T_m$ . The diffused phase transition occurs due to the presence of different Curie points of the polar nanoregions; the composition fluctuation at the A-site of the examined compositions is responsible for this phenomenon. It is proposed that for typical relaxor-like PMN, the local Curie points ( $\theta$ ) of PNRs follow the Gaussian type distribution above the mean Curie temperature ( $T_0$ ).<sup>7</sup> The distribution function can be written as

$$\varphi = \frac{1}{\sqrt{2\pi\delta^2}} e^{-\frac{(\theta-T_0)^2}{2\delta^2}}, \quad (15)$$

where the standard deviation ( $\delta$ ) denotes the diffuseness of the permittivity curve. The states of polarization of these regions are separated by the energy barrier.<sup>17</sup> At higher temperature, the energy of the barrier becomes lower, and the relaxators are able to surpass the barrier, but those that have Curie points equal to temperature  $T$  will contribute to dielectric response.<sup>7</sup> The number of the contributing relaxators is given by

$$n = \frac{N\Delta T}{\sqrt{2\pi\delta^2}} e^{-\frac{(T-T_0)^2}{2\delta^2}}, \quad (16)$$

where  $N$  is the maximum number of contributing relaxators,  $T_0$  is the mean Curie temperature, and  $\Delta T$  is the difference between the local Curie points of the relaxators and  $T$ . For the higher concentration of  $\text{Rb}^{1+}$  in the NBT matrix, the local Curie points of the PNRs are distributed far from the mean value ( $T_0$ ), which enlarges the standard deviation and the permittivity peak becomes more broad near  $T_m$ . Usually, below  $T_B$ , two other peaks exist in the temperature dependent dielectric curve ( $\epsilon'$ ); the first one is associated with  $T_m$ , and the second is associated with the depolarization temperature ( $T_d$ ). These two peaks are also observed in the Rb substituted NBT, which are shown in Fig. 7(a).  $T_m$  values of the  $\text{Na}_{0.5-x}\text{Rb}_x\text{Bi}_{0.5}\text{TiO}_3$  compositions are found to decrease with the increase in mol. % of Rb. The plot of  $T_m$  vs size variance is shown in Fig. 7(b). Along with the decrease in  $T_m$ , the dielectric constant at this temperature also decreases with the substitution of  $\text{Rb}^{1+}$ . These observations indicate that the substitution of  $\text{Rb}^{1+}$  disrupts the long range ferroelectric order. The A-site disorder enhances with  $\text{Rb}^{1+}$  due to different radii and polarizabilities from  $\text{Na}^{1+}$  and  $\text{Bi}^{3+}$ .<sup>9,18</sup> Its effect is strongly manifested by lower  $T_m$ ,  $\epsilon'$  and polarization values of RB3 and RB4. The decrease in  $T_d$  shows that the ferroelectric nature withstands for a

shorter temperature region. The variation of  $T_d$  with the cation size variance is shown in Fig. 7(b). On the basis of the experimental results, a general relation can be established among  $T_m$ ,  $T_d$ , and  $T_B$ . Usually, the NBT-based systems with the increase in the substitution with different cations exhibit lower  $T_m$ , lower  $T_d$ , and higher  $T_B$ . This relation may not be applicable for the optimized composition (especially, in the case of the lower concentration of substitution), where the system shows higher polarization and dielectric constant.

## B. Effect of the cation size variance on the relaxation time

The relaxation phenomenon tells about the slowing down of the response of the dipoles when the external signal is removed. Usually, the relaxation is studied on the dependency of the real and imaginary parts of the dielectric constant with frequency (frequency domain approach). The response of the polarization ( $P$ ) to the applied electric field ( $E_0 \cos \omega t$ , where  $E_0$  and  $\omega$  are the amplitude and frequency of the applied electric field, respectively) is shown as follows:

$$P = (\epsilon_{r\infty} - 1)\epsilon_0 E_0 \cos \omega t + \frac{(\epsilon_{rs} - \epsilon_{r\infty})E_0 \cos \omega t}{1 + \omega^2 \tau_0^2} + \frac{(\epsilon_{rs} - \epsilon_{r\infty})\omega \tau_0 E_0 \sin \omega t}{1 + \omega^2 \tau_0^2}, \quad (17)$$

where  $\epsilon_{r\infty}$ ,  $\epsilon_0$ ,  $\epsilon_{rs}$ , and  $\tau_0$  are the dielectric constant at higher frequency, dielectric constant at vacuum, dielectric constant at lower frequency, and relaxation time of a single entity, respectively. The first term on the right-hand side of Eq. (17) is associated with electronic and atomic polarizations. The second and third terms are associated with the orientational polarization; the third term lags by  $90^\circ$  with the electric field. After the separation of the real and imaginary parts of permittivity ( $\epsilon'$  and  $\epsilon''$ , respectively), it can be proved that the maximum of the imaginary part of permittivity occurs at  $\omega = \frac{1}{\text{relaxation time}(\tau_0)}$ , which indicates the maximum energy loss at this frequency. Similar to the  $\epsilon''$  spectrum, the  $Z''$  spectrum also provides information about the relaxation phenomena.<sup>19</sup> Figures 8 and 9 depict the frequency dependent  $Z''$  spectra at temperatures from 200  $^{\circ}\text{C}$  to 500  $^{\circ}\text{C}$  of RB0 and RB4. It is observed that with decreasing temperature, the maximum of  $Z''$  shifts toward the lower frequency



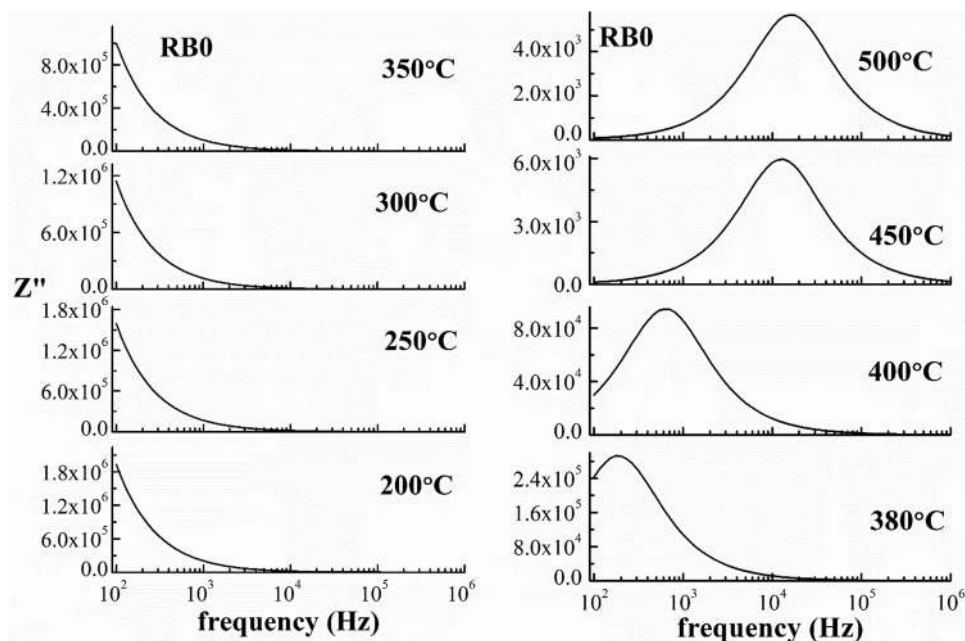


FIG. 8. Imaginary part of the impedance spectra at various temperatures of RB0. The symmetric peaks are noticed for this composition at the higher temperature.

side, which denotes the higher relaxation time of the relaxators. This also describes the gradual decrease in the response time of the relaxators with respect to the applied signal at the lower temperature region. At temperatures below 500 °C, the maximum of the  $Z''$  spectrum of RB4 becomes broad and asymmetric. The distribution of the relaxation times of the polar nanoregions is the most possible reason

behind the broadness of the maxima of the  $Z''$  spectra. Similar to the diffused permittivity peak, impedance spectra also show a broad peak, which indicates that PNRs possess not only dissimilar Curie temperature but also dissimilar relaxation times.<sup>7,20</sup> The broadness of the  $Z''$  spectrum of RB4 (below  $T_B$ ) also supports this fact. The Havriliak–Negmi relaxation equation is adopted to analyze

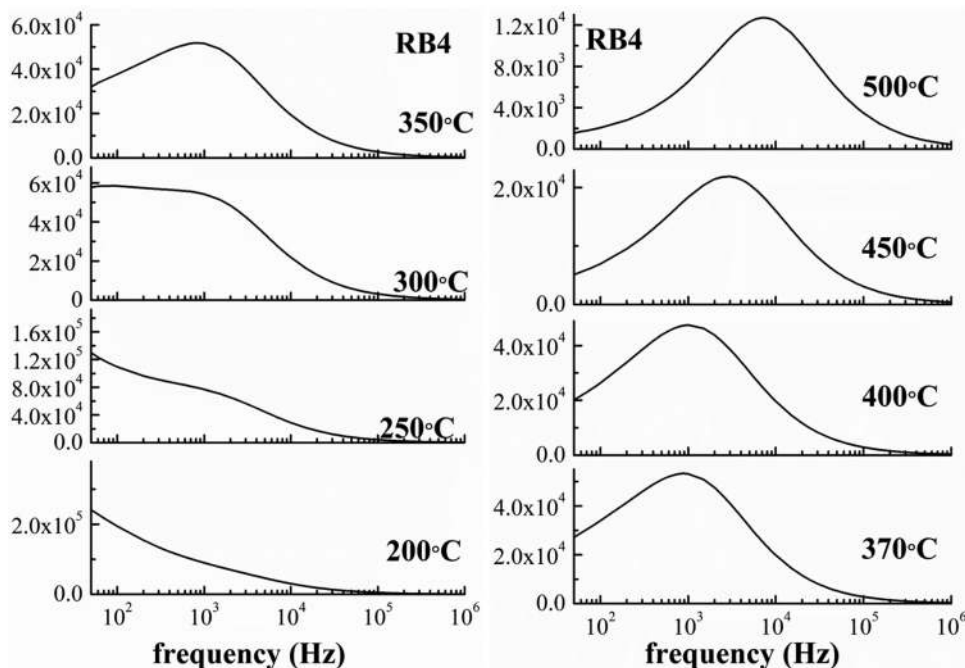


FIG. 9. Imaginary part of the impedance spectra at various temperatures of RB4. Asymmetry is observed in the peaks of the curves for this composition. This reveals the distribution of the relaxation times of the PNRs, which was mentioned by Kirillov and Isupov.<sup>7</sup> Asymmetry of the  $Z''$  maxima vanish above 450 °C.

quantitatively the distribution of the relaxation time and the dielectric dispersion curve,<sup>21</sup>

$$\epsilon^* = \epsilon_\infty + \frac{\epsilon_s - \epsilon_\infty}{\{1 + (i\omega\tau)^\alpha\}^\beta}, \quad (18)$$

where  $\epsilon^*$  is the complex dielectric constant,  $\epsilon_s$  is the dielectric constant at lower frequency,  $\epsilon_\infty$  is the dielectric constant at higher frequency,  $\tau$  is the characteristic relaxation time,  $\omega$  is equal to  $2\pi \times f$  ( $f$ =applied frequency), and  $\alpha$  ( $0 < \alpha \leq 1$ ) and  $\beta$  ( $0 < \beta \leq 1$ ) are associated with the distribution of relaxation times and the shape of the dispersion curve, respectively. The above equation is a modification of the Debye equation with the addition of two parameters, and it transforms into Debye equation when  $\alpha = \beta = 1$ . The temperature dependent real and imaginary parts of permittivity data are fitted

with real and imaginary parts of the above equation. Here, the fitted experimental data of the real part of permittivity ( $\epsilon'$ ) of RB0 and RB4 are shown in Figs. 10 and 11. The variations of  $\alpha$  and  $\beta$  as a function of temperature are shown in Figs. 12(a) and 12(b). As shown in figure, the values of  $\alpha$  of RB4 exist in the range of 0.58–0.68; this implies that RB4 has multiple relaxation times at the range of the studied temperature.<sup>22</sup> The value of another parameter  $\beta$  rises from 0.53 to 0.62 with the increase in temperature from 300 to 500 °C. This proves the more asymmetrical distribution of relaxation times of RB4 below 450 °C.<sup>22</sup> The broadness of the  $Z''$  spectra also provide evidence for it. On the other side, the values of  $\alpha$  of RB0 is found to be in the range of 0.79–0.87, which denotes that pure NBT also does not possess single relaxation time, but comparatively in lesser polydispersive nature than RB4. The obtained  $\beta$  values of this composition are observed in the range of 0.85–0.95

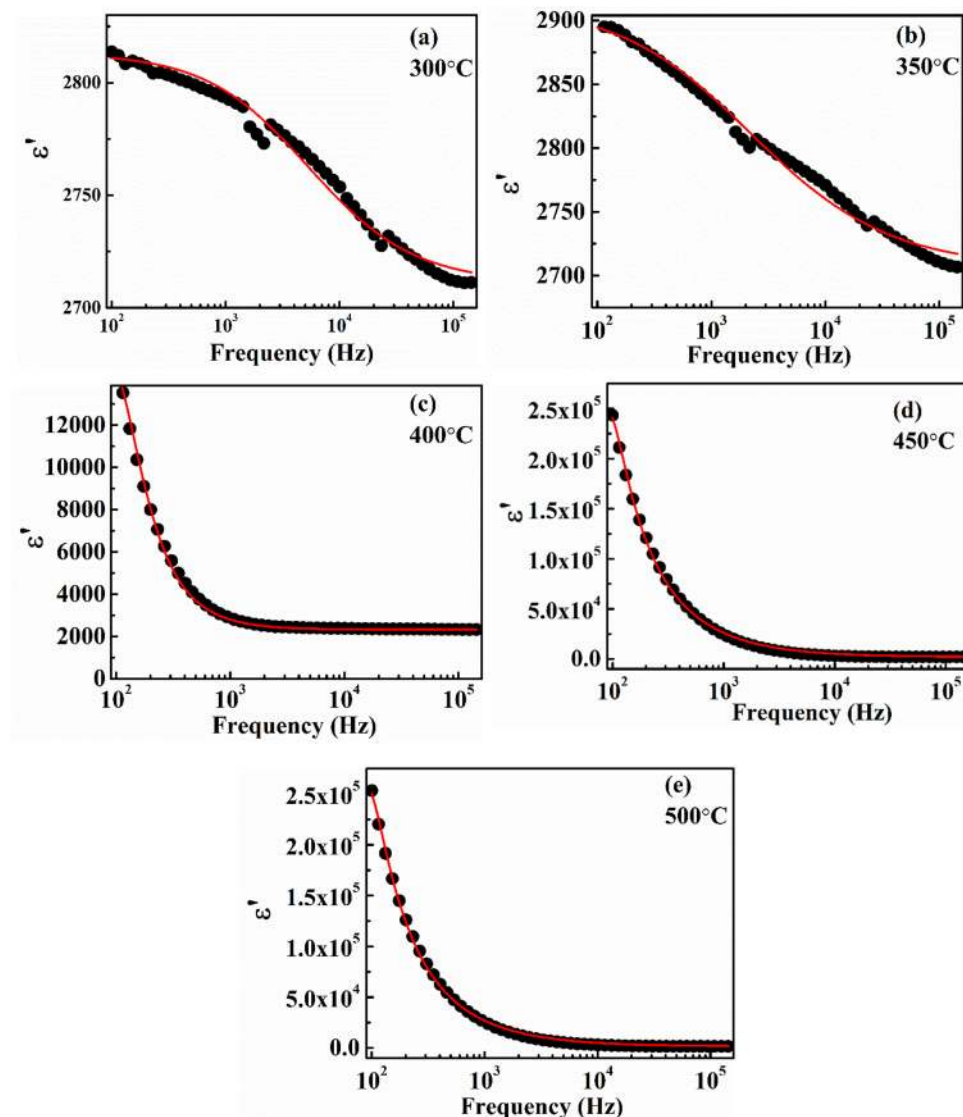


FIG. 10. The graph of the real part of the permittivity of RB0 as a function of frequency at (a) 300 °C, (b) 350 °C, (c) 400 °C, (d) 450 °C, and (e) 500 °C. The experimental data are shown by filled circles. The fits of the Havriliak–Negami relaxation equation is shown by red colored solid curves.

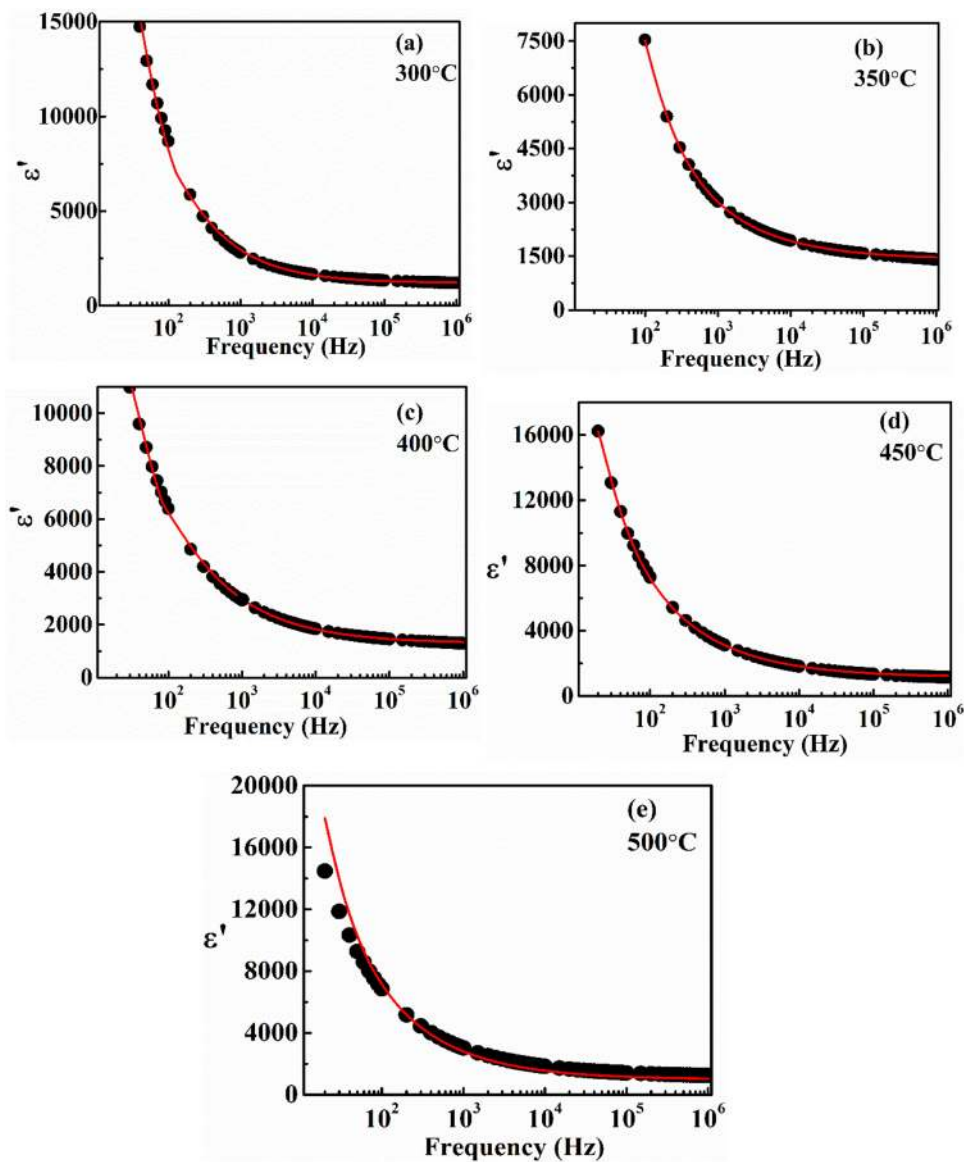


FIG. 11. The graph of the real part of permittivity of RB4 as a function of frequency at (a) 300 °C, (b) 350 °C, (c) 400 °C, (d) 450 °C, and (e) 500 °C. The experimental data are shown by filled circles. The fits of the Havriliak–Negmi relaxation equation is shown by red colored solid curves.

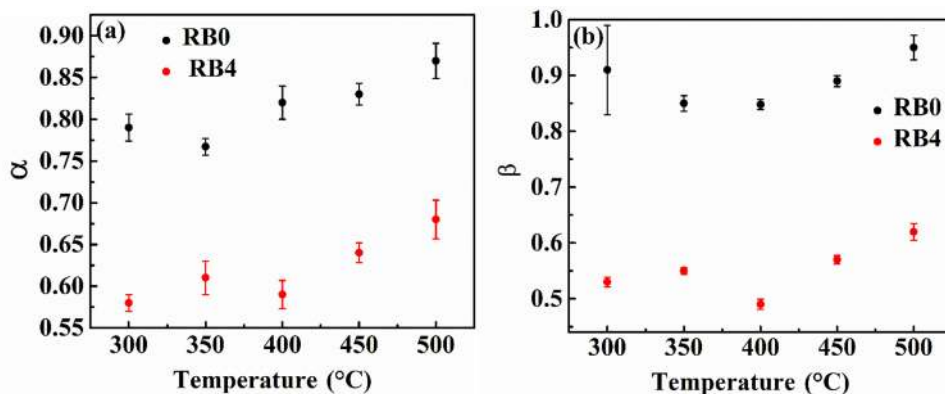


FIG. 12. The variations of the fitting parameters (a)  $\alpha$  and (b)  $\beta$  as a function of temperature of Rb0 and RB4.

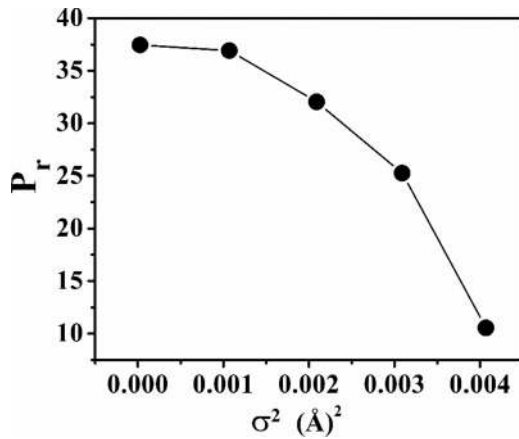


FIG. 13. The variation of the remanent polarization ( $P_r$ ) with respect to  $\sigma^2$  for  $\text{Na}_{0.5-x}\text{Rb}_x\text{Bi}_{0.5}\text{TiO}_3$  compositions. The unit of  $P_r$  is  $\mu\text{C}/\text{cm}^2$ .

with the increasing temperature. This observation shows the almost symmetrical distribution of the relaxation times at higher temperatures (above  $T_m$ ).

### C. Effect of the cation size variance on the remanent polarization

The A-site cation radius mismatch leads to additional displacement in  $\text{O}^{2-}$  positions at apical and planer ions, which affect the polarization of the compound. The gradual increase in the concentration of  $\text{Rb}^+$  reduces the remanent polarization ( $P_r$ ), which has been observed from the polarization vs electric field curve.<sup>5</sup>  $P_r$  is plotted with respect to  $\sigma^2$  (see Fig. 13). The reason behind the reduction in the value of  $P_r$  is the restoration of the nanodomains at the random state while the external electric field is removed.<sup>23</sup> The disruption of the long range ferroelectric order is presumably attributed to the disorder at the A-site. This result indicates about the relationship between  $T_B$  and  $P_r$ , as  $T_B$  also shows dependency on the cation size disparity. The PNRs nucleate at  $T_B$ , and their polarization is the consequence of displacements of the ions and

rotation of the  $\text{BO}_6$  octahedra (at lower temperature) from the higher symmetric structure. The correlation among the PNRs and their polarizations are influenced by the A-site radius mismatch, and the outcomes are noticed in terms of enhanced broadness in the dielectric response in the vicinity of  $T_m$  and reduced  $P_r$ , which are the characteristic features of RFs. The effect of substitution is observed in some of the lead-based systems; the substitution of La in  $\text{Pb}[\text{Zr}_x\text{Ti}_{1-x}]\text{O}_3$  (PZT) suppresses the Zr/Ti displacement and destroys the long range ferroelectric order and establishes the relaxor nature.<sup>24</sup> Furthermore, the relationship between  $T_B$  and  $P_r$  is verified in other NBT-based A-site disordered systems.  $T_B$  vs  $P_r$  of 12 compositions (NBT-based A-site disordered systems and some solid solutions) are plotted on the basis of literature and our group results, which is shown in Fig. 14(a). These materials contain the substitution at either the  $\text{Na}^{1+}$  site or the  $\text{Bi}^{3+}$  site. The values of  $P_r$  and  $T_B$  of the compositions are listed in Table I.

The obtained experimental data are fitted by using the polynomial equation with one variable. The obtained equation is as follows:

$$T_B = (485.267 \pm 10.970) + (0.976 \pm 1.240)P_r - (0.077 \pm 0.028)P_r^2. \quad (19)$$

As shown in Fig. 14(b), a linear relation between  $T_B$  and  $P_r^2$  is found. The data are fitted, and the obtained equation is as follows:

$$T_B = -(0.055 \pm 0.005)P_r^2 + (439.290 \pm 3.985). \quad (20)$$

It is worthy to mention here that a similar type of linear relation but with a positive slope exists for displacive ferroelectrics. Abrahams *et al.*<sup>29</sup> showed the linear relation between  $T_c$  and square of the spontaneous polarization ( $P_S^2$ ) for displacive ferroelectrics, which was theoretically established by Lines.<sup>30</sup> It was experimentally proved that  $T_c$  and  $P_S$  both are related to the displacement of Ti or Nb of the  $\text{BaTiO}_3$ ,  $\text{NaNbO}_3$ ,  $\text{KNbO}_3$ , and  $\text{PbTiO}_3$  ferroelectrics.<sup>29</sup> Our current experimental study also shows the similarities between the transition temperature and polarization of the relaxor and displacive ferroelectrics, and it can be inferred that  $T_B$  and  $P_r$  of the RFs are associated with the displacement of the ions and the rotation of the octahedron. It is worthwhile to mention here that

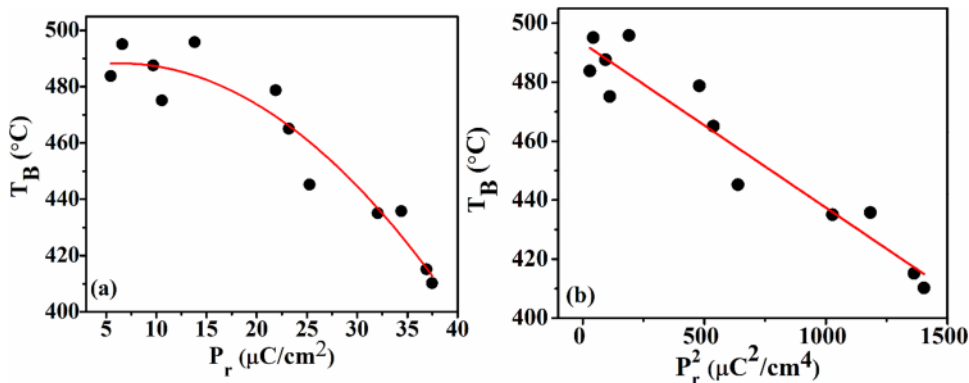


FIG. 14. (a) The graph of  $T_B$  vs  $P_r$  of the NBT-based A-site disorder ferroelectrics and solid solutions. The red colored curve denotes the fitted Eq. (18). (b) The plot of  $T_B$  vs  $P_r^2$  of same compositions. The data are fitted by a linear equation [Eq. (19)], which is shown by a red colored straight line.

**TABLE I.** The values of  $P_r$  and  $T_B$  of some NBT-based A-site disordered systems and solid solutions.

$P_r$ ( $\mu\text{C}/\text{cm}^2$ )	$T_B$ ( $^\circ\text{C}$ )	Compound
37.45	410.24	$\text{Na}_{0.5}\text{Bi}_{0.5}\text{TiO}_3^{\text{a}}$
36.91	415.16	$\text{Na}_{0.49}\text{Rb}_{0.01}\text{Bi}_{0.5}\text{TiO}_3^{\text{a}}$
32.044	435.10	$\text{Na}_{0.48}\text{Rb}_{0.02}\text{Bi}_{0.5}\text{TiO}_3$
25.264	445.25	$\text{Na}_{0.47}\text{Rb}_{0.03}\text{Bi}_{0.5}\text{TiO}_3$
10.55	475.13	$\text{Na}_{0.46}\text{Rb}_{0.04}\text{Bi}_{0.5}\text{TiO}_3$
6.60	495.14	$\text{Na}_{0.5}\text{Bi}_{0.45}\text{Eu}_{0.05}\text{TiO}_3^{\text{b}}$
23.19	465.10	$\text{Na}_{0.5}\text{Bi}_{0.48}\text{Ho}_{0.02}\text{TiO}_3^{\text{c}}$
13.81	495.85	$\text{Na}_{0.5}\text{Bi}_{0.47}\text{Ho}_{0.03}\text{TiO}_3$
34.40	435.82	$(\text{Na}_{0.5}\text{Bi}_{0.5})_{0.96}\text{Ba}_{0.04}\text{TiO}_3^{\text{d,e}}$
21.89	478.74	$\text{Na}_{0.3}\text{K}_{0.2}\text{Bi}_{0.5}\text{TiO}_3^{\text{f}}$
5.45	483.84	$\text{Na}_{0.25}\text{K}_{0.25}\text{Bi}_{0.5}\text{TiO}_3^{\text{g}}$
9.68	487.59	$0.94(\text{Na}_{0.4}\text{K}_{0.1}\text{Bi}_{0.5}\text{TiO}_3)-0.06$ $(\text{Ba}_{0.85}\text{Ca}_{0.15}\text{Ti}_{0.9}\text{Zr}_{0.1}\text{O}_3)^{\text{h}}$

<sup>a</sup>Reference 5.<sup>b</sup>Reference 25.<sup>c</sup>Reference 26.<sup>d</sup>Reference 27.<sup>e</sup>Reference 28.<sup>f</sup>Figure S1 in the supplementary material.<sup>g</sup>Figure S2 in the supplementary material.<sup>h</sup>Figure S3 in the supplementary material.

the variation of  $P_r$  with temperature in RFs is different from the NFs. The  $P_r$  value vanishes not at  $T_B$  but at the ferroelectric-to-relaxor transition temperature ( $T_{F-R}$ ), which is lower than  $T_B$ .<sup>31</sup> The dipole moments of the PNRs fluctuate between the equivalent polarization states, and the dynamical character persists above  $T_m$ , which is revealed through the diffuse nature of the dielectric curve.<sup>17,32</sup> Therefore, it is difficult to provide a similar reason behind the relationship between  $T_B$  and  $P_r$  like NFs. However, on the basis of the observed results, it can be concluded that the enhanced correlation among polarizations of the PNRs and their randomness in the absence of the external electric field increases the  $T_B$  and reduces the  $P_r$ , respectively, in the A-site substituted NBT-based systems.

#### IV. CONCLUSION

The mismatch among the radii of different cations in the Rb substituted NBT creates the local disorder, which is responsible for diffused phase transition and smaller value of  $P_r$ . Based on the observations, it is clear that the size variance is one of the reasons to tune the transition temperature in RFs. The increased A-site cation disparity with the higher concentration of the substituted ions diminishes the normal ferroelectric behavior and causes an increment in the nucleation temperature of the PNRs ( $T_B$ ). The possible reason behind the increment of  $T_B$  is the correlations among the PNRs, which are estimated through the temperature dependent order parameter. The possession of the dissimilar relaxation times along with dissimilar Curie temperatures of the PNRs is observed from the impedance studies and the temperature

dependence parameters estimated from the Havriliak–Negmi relaxation equation. The linear relation between  $T_B$  and  $P_r^2$  with negative slope is noticed for different lead free NBT-based systems. It is found that the relation is followed well by the A-site substituted systems rather than the solid solutions of two perovskites. This relation can be experimentally proved from the temperature dependent refractive index and the polarization vs electric field measurements of the collected compounds. However, a theoretical study is required for the lead free A-site disorder systems to confirm this relationship. This work will be helpful to select the material to attain desired  $P_r$  and transition temperature; especially, it will help to design lead free ferroelectrics for energy storage applications.

#### SUPPLEMENTARY MATERIAL

See the [supplementary material](#) for the Burns temperature and polarization data of similar type of materials from our lab for providing better understating to the readers.

#### ACKNOWLEDGMENTS

S.A. gratefully acknowledges financial support provided by UGC-DAE (No. CRS-M-250) and CSIR-EMRII (Ref. No. 0194/NS), India, to carry out this work. K.B. acknowledges DST-INSPIRE, India (Fellowship Code No. IF160462), for financial assistance.

#### REFERENCES

- L. M. Rodriguez-Martinez and J. P. Attfield, "Cation disorder and size effects in magnetoresistive manganese oxide perovskites," *Phys. Rev. B* **54**, R15622 (1996).
- D. C. Sinclair and J. P. Attfield, "The influence of A-cation disorder on the Curie temperature of ferroelectric  $\text{ATiO}_3$  perovskites," *Chem. Commun.* **16**, 1497 (1999).
- T. Wei, C. Zhu, K. F. Wang, H. L. Cai, J. S. Zhu, and J.-M. Liu, "Influence of A-site codoping on ferroelectricity of quantum paraelectric  $\text{SrTiO}_3$ ," *J. Appl. Phys.* **103**, 124104 (2008).
- A. Berenov, F. Le Goupil, and N. Alford, "Effect of ionic radii on the Curie temperature in  $\text{Ba}_{1-x}\text{Sr}_x\text{Ca}_y\text{TiO}_3$  compounds," *Sci. Rep.* **6**, 28055 (2016).
- K. Banerjee, S. B. Alvi, A. K. Rengan, and S. Asthana, "Investigation on the discharge energy storage density of the Rb substituted  $\text{Na}_{0.5}\text{Bi}_{0.5}\text{TiO}_3$  relaxor ferroelectric and its suitability for the orthopedic application," *J. Am. Ceram. Soc.* **102**, 6802 (2019).
- J. P. Attfield, "A simple approach to lattice effects in conducting perovskite-type oxides," *Chem. Mater.* **10**, 3239 (1998).
- V. V. Kirillov and V. A. Isupov, "Relaxation polarization of  $\text{PbMg}_{1/3}\text{Nb}_{2/3}\text{O}_3$  (PMN)—A ferroelectric with a diffused phase transition," *Ferroelectrics* **5**, 3 (1973).
- K. Uchino and S. Nomura, "Critical exponents of the dielectric constants in diffused-phase-transition crystals," *Ferroelectrics* **44**, 55 (1982).
- G. A. Samara, "Ferroelectricity revisited—Advances in materials and physics," *Solid State Phys.* **56**, 239 (2001).
- D. Viehland, J. F. Li, S. J. Jang, L. E. Cross, and M. Wuttig, "Dipolar-glass model for lead magnesium niobate," *Phys. Rev. B* **43**, 8316 (1991).
- D. Sherrington and S. Kirkpatrick, "Solvable model of a spin-glass," *Phys. Rev. Lett.* **35**, 1792 (1975).
- D. Viehland, S. J. Jang, L. E. Cross, and M. Wuttig, "Deviation from Curie-Weiss behavior in relaxor ferroelectrics," *Phys. Rev. B* **46**, 8003 (1992).
- A. A. Bokov and Z.-G. Ye, "Phenomenological description of dielectric permittivity peak in relaxor ferroelectrics," *Solid. State Commun.* **116**, 105 (2000).

- <sup>14</sup>A. A. Bokov, Y. H. Bing, W. Chen, Z.-G. Ye, S. A. Bogatina, I. P. Raevski, S. I. Raevskaya, and E. V. Sahkar, "Empirical scaling of the dielectric permittivity peak in relaxor ferroelectrics," *Phys. Rev. B* **68**, 052102 (2003).
- <sup>15</sup>Z.-Y. Cheng, R. S. Katiyar, X. Yao, and A. Guo, "Dielectric behavior of lead magnesium niobate relaxors," *Phys. Rev. B* **55**, 8165 (1997).
- <sup>16</sup>M. Wolters and A. J. Burggraaf, "Relaxational polarization and diffuse phase transitions of LA-substituted Pb(Zr,Ti)O<sub>3</sub>-ceramics," *Mater. Res. Bull.* **10**, 417 (1975).
- <sup>17</sup>D. Viehland, S. J. Jang, L. E. Cross, and M. Wuttig, "Freezing of the polarization fluctuations in lead magnesium niobate relaxors," *J. Appl. Phys.* **68**, 2916 (1990).
- <sup>18</sup>J.-K. Lee, K. S. Hong, C. K. Kim, and S.-E. Park, *J. Appl. Phys.* **91**, 4538 (2002).
- <sup>19</sup>S. Dutta, R. N. P. Choudhary, P. K. Sinha, and A. K. Thakur, "Microstructural studies of (PbLa)(ZrTi)O<sub>3</sub> ceramics using complex impedance spectroscopy," *J. Appl. Phys.* **96**, 1607 (2004).
- <sup>20</sup>O. Raymond, R. Font, N. S. Almodovar, J. Portelles, and J. M. Siqueiros, "Frequency-temperature response of ferroelectromagnetic PbFe<sub>1/2</sub>Nb<sub>1/2</sub>O<sub>3</sub> ceramics obtained by different precursors. Part II. Impedance spectroscopy characterization," *J. Appl. Phys.* **97**, 084108 (2005).
- <sup>21</sup>S. Havriliak and S. Negami, "A complex plane representation of dielectric and mechanical relaxation processes in some polymers," *Polymer* **8**, 161 (1967).
- <sup>22</sup>K. C. Kao, *Dielectric Phenomena in Solids* (Elsevier, 2004).
- <sup>23</sup>Z. G. Ye, "Relaxor ferroelectric complex perovskites: Structure, properties and phase transitions," in *In Key Engineering Materials* (Trans Tech Publications, 1998), Vol. 155, pp. 81–122.
- <sup>24</sup>S. Teslic, T. Egami, and D. Viehland, "Local atomic structure of PZT and PLZT studied by pulsed neutron scattering," *J. Phys. Chem. Solids* **57**, 1537 (1996).
- <sup>25</sup>K. R. Kandula, S. S. K. Raavi, and S. Asthana "Dielectric, ferroelectric, and photoluminescence properties of lead free Eu substituted Na<sub>0.5</sub>Bi<sub>0.5</sub>TiO<sub>3</sub>" (unpublished).
- <sup>26</sup>A. Kumar and S. Asthana "Enhanced thermally stable energy storage density, and thermally stable capacitance for high temperature electronic (HTE) device applications in the holmium substituted Na<sub>0.5</sub>Bi<sub>0.5</sub>TiO<sub>3</sub>" (unpublished).
- <sup>27</sup>E. Dul'kin, E. Mojaev, and M. Roth, "Detecting the Burns temperature in Na<sub>0.5</sub>Bi<sub>0.5</sub>TiO<sub>3-x</sub>BaTiO<sub>3</sub> lead-free relaxor ferroelectrics by means of acoustic emission," *Europhys. Lett.* **124**, 57001 (2018).
- <sup>28</sup>Q. Xu, S. Chen, W. Chen, S. Wu, J. Zhou, H. Sun, and Y. Li, "Synthesis and piezoelectric and ferroelectric properties of (Na<sub>0.5</sub>Bi<sub>0.5</sub>)<sub>1-x</sub>Ba<sub>x</sub>TiO<sub>3</sub> ceramics," *Mater. Chem. Phys.* **90**, 111 (2005).
- <sup>29</sup>S. C. Abrahams, S. K. Kurtz, and P. B. Jamieson, "Atomic displacement relationship to Curie temperature and spontaneous polarization in displacive ferroelectrics," *Phys. Rev.* **172**, 551 (1968).
- <sup>30</sup>M. E. Lines, "Statistical theory for displacement ferroelectrics," *Phys. Rev.* **177**, 797 (1969).
- <sup>31</sup>W. Jo, J. Daniels, D. Damjanovic, W. Kleemann, and J. Rödel, "Two-stage processes of electrically induced ferroelectric to relaxor transition in 0.94(Bi<sub>1/2</sub>Na<sub>1/2</sub>)TiO<sub>3</sub>-0.06BaTiO<sub>3</sub>," *Appl. Phys. Lett.* **102**, 192903 (2013).
- <sup>32</sup>C. W. Ahn, C.-H. Hong, B.-Y. Choi, H.-P. Kim, H.-S. Han, Y. Hwang, W. Jo, K. Wang, J.-F. Li, J.-S. Lee, and I. W. Kim, "A brief review on relaxor ferroelectrics and selected issues in lead-free relaxors," *J. Korean Phys. Soc.* **68**, 1481 (2016).